BIOCHEMISTRY
including biophysical chemistry & molecular biology

Article

pubs.acs.org/biochemistry

# Long Time Scale GPU Dynamics Reveal the Mechanism of Drug Resistance of the Dual Mutant I223R/H275Y Neuraminidase from H1N1-2009 Influenza Virus

Christopher J. Woods,*[,†] Maturos Malaisree,[†] Naruwan Pattarapongdilok,[‡] Pornthep Sompornpisut,[§] Supot Hannongbua,[§] and Adrian J. Mulholland*[,†]

[†]Centre for Computational Chemistry, School of Chemistry, University of Bristol, Bristol BS8 1TS, U.K.

[‡]Science Program, Faculty of Education, Bansomdejchaopraya Rajabhat University, Bangkok 10600, Thailand

[§]Computational Chemistry Unit Cell, Department of Chemistry, Faculty of Science, Chulalongkorn University, Bangkok 10330, Thailand

Supporting Information

**ABSTRACT:** Multidrug resistance of the pandemic H1N1-2009 strain of influenza has been reported due to widespread treatment using the neuraminidase (NA) inhibitors, oseltamivir (Tamiflu), and zanamivir (Relenza). From clinical data, the single I223R (IR[1]) mutant of H1N1-2009 NA reduced efficacy of oseltamivir and zanamivir by 45 and 10 times,[1] respectively. More seriously, the efficacy of these two inhibitors against the double mutant I223R/H275Y (IRHY[2]) was significantly reduced by a factor of 12 374 and 21 times, respectively, compared to the wild-type.[2] This has led to the question of why the efficacy of the NA inhibitors is reduced by the occurrence of these mutations and, specifically, why the efficacy of oseltamivir against the double mutant IRHY was significantly reduced, to the point where oseltamivir has become an ineffective treatment. In this study, 1 $\mu$s of molecular dynamics (MD) simulations was performed to answer these questions. The simulations, run using graphical processors (GPUs), were used to investigate the effect of conformational change upon binding of the NA inhibitors oseltamivir and zanamivir in the wild-type and the IR and IRHY mutant strains. These long time scale dynamics simulations demonstrated that the mechanism of resistance of IRHY to oseltamivir was due to the loss of key hydrogen bonds between the inhibitor and residues in the 150-loop. This allowed NA to transition from a closed to an open conformation. Oseltamivir binds weakly with the open conformation of NA due to poor electrostatic interactions between the inhibitor and the active site. The results suggest that the efficacy of oseltamivir is reduced significantly because of conformational changes that lead to the open form of the 150-loop. This suggests that drug resistance could be overcome by increasing hydrogen bond interactions between NA inhibitors and residues in the 150-loop, with the aim of maintaining the closed conformation, or by designing inhibitors that can form a hydrogen bond to the mutant R223 residue, thereby preventing competition between R223 and R152.

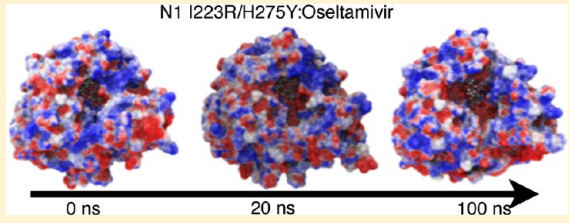


The H1N1-2009 influenza virus (colloquially called "swine flu") has spread globally by human-to-human transmission since April 2009.[3] This new, highly adaptive virus is derived from different gene segments of swine, avian, and human influenza.[4] Within a few months of its appearance, the H1N1-2009 strain became the first influenza pandemic of the 21st century. Antiviral drugs that target the neuraminidase (NA) enzyme of influenza have been used successfully to treat H1N1-2009 infection. However, widespread use of these drugs has led to a series of mutations in NA that reduce the drugs' efficacy. The aim of this study is to use computer simulation to understand, at a molecular level, how point mutations in NA can lead to drug resistance. The hope is this could provide insight that would lead to the development of the next generation of antiviral treatments of influenza.

## BACKGROUND

**Conformational Substates of NA.** There are two phylogenetically distinct groups of NA: group 1 (N1, N4, N5, and N8) and group 2 (N2, N3, N6, N7, and N9). NA from H1N1-2009 belongs to group 1. X-ray structures[5] of NA show that group 1 NA is structurally distinct from group 2. Group 1 NA has a flexible 150-loop (residues 147−152) that can exist in two stable conformations: open and closed. In contrast, the 150-loop in group 2 NA exists only in the closed conformation. The current commercial antiviral treatments of influenza that target NA are oseltamivir (commercially called Tamiflu[6]) and zanamivir (commercially called Relenza[7]). These NA inhibitors were developed using information from X-ray structures of group 2 NA, where the protein crystallized in the closed conformation. These inhibitors were designed to bind to the closed form of the enzyme, to mimic the natural substrate, sialic acid, to prevent NA functioning during the propagation step of viral replication. Influenza virus uses NA to cleave the terminal sialic

Received: May 1, 2012
Revised: May 10, 2012
Published: May 10, 2012

  

acid, thereby allowing release of progeny viruses from the host cells.[8] As the active site of NA in all strains is highly conserved,[8] antiviral drugs developed for group 2 can be used to treat patients infected by group 1 strains of the virus and so are effective treatments for H1N1-2009.

X-ray crystallography provides structures of the apo form group 1 NAs that are predominantly in the open conformation.[5,9,10] These studies have also shown that group 1 NAs can bind oseltamivir in either the open or closed conformation, depending on the soaking conditions.[5] Soaking of oseltamivir for 150 min into preformed crystals of the open form of N1 NA shows no large conformational changes, with the 150-loop remaining in the open conformation. However, when the N1 crystals are soaked with a higher concentration of oseltamivir, the 150-loop undergoes a conformational change to a closed structure that is similar to that seen in group 2 NAs.[5] This suggests that the open form of the loop is more stable in the unbound apoenzyme, while binding of the inhibitor induces a conformational change to the closed form. This suggestion is supported by a computational study that calculated binding free energies of inhibitors to the closed and open forms of H5N1 NA using MM/PBSA.[11] Binding free energies were calculated from a series of 3 ns dynamics simulations of a five ligands binding to the open and closed form of NA from the H5N1 strain. The results showed that oseltamivir had a strong preference to bind to the closed form of NA (absolute binding free energy of $-8.5$ kcal mol$^{-1}$ for the closed form, compared to $+12.4$ kcal mol$^{-1}$ for the open form). In contrast, zanamivir was shown to be able to bind to either conformation (absolute binding free energy of $-13.3$ kcal mol$^{-1}$ for closed and $-13.0$ kcal mol$^{-1}$ for open).

Genetic analysis and crystallographic techniques have been used to gain insight into the molecular properties of the H1N1-2009 strain of influenza. The hemagglutinin (HA) protein from H1N1-2009 was found to have antigenic similarity with the H1N1-1918 "Spanish flu" strain.[12] In contrast, the neuraminidase (NA) protein from H1N1-2009 showed structural differences compared to NA from the normal N1 strains. It was surprising to observe that the apo form of NA from H1N1-2009 crystallized with a closed form of the 150-loop and with no 150-cavity.[13] This is in contrast to all other X-ray structures of other N1 variants that show an open structure of the apo form. However, crystallization of only the closed form of the apo H1N1-2009 structure does not mean that the open form does not exist in solution. Explicit solvent molecular dynamics (MD) simulations[14] of NA from H5N1 for 40 ns showed that the 150-loop opened more and was more flexible than was observed in the X-ray structure. The simulations also showed an opening of the adjacent 430-loop that expanded the cavity next to the active site.[14] To enhance conformational sampling, implicit solvent Generalized Born (GB MD) simulations of the N1 and N9 NA were used to study the dynamical differences in the 150-loop and 430-loop. The simulations also suggested that this loop conformation may be more flexible than observed in the crystal structures.[15] Further, recent explicit solvent 100 ns MD simulations[16] of the tetramer of the wild-type and variants of H1N1-2009 show that the 150-loop opens.

**Appearance of Drug-Resistant Mutations.** Oseltamivir and zanamivir are used widely for the treatment of influenza, while a new NA inhibitor, peramivir, has recently been authorized by the FDA for patients infected by the H1N1-2009 strain.[17] Because of the widespread use of these NA inhibitors, several mutant strains of H1N1-2009 have appeared that reduce the binding efficacy of the compounds and thus cause drug resistance. A common mutation in the N1 subtype is H275Y (hereafter called "HY") which can still be treated by inhaled zanamivir but is resistant to oseltamivir.[18,19] Since the large-scale outbreak of influenza H1N1-2009, several cases of this HY, oseltamivir-resistant strain have been detected, causing almost 500 reported infections.[20] Recently, two new NA mutants, I223R[1,21] (hereafter called "IR") and I223R/H275Y[2] (hereafter called "IRHY"), have been reported with multidrug resistance. Recent data suggest that the "IR" mutation has the potential to spread into the general human population.[22] From clinical data, the efficacy of oseltamivir, zanamivir, and peramivir against the IR mutant was reduced, with a 45, 10, and 7 times increase in resistance,[1] respectively, compared to the wild-type. Of more concern, the efficacy of these three NA inhibitors against the double mutant, IRHY, was significantly reduced compared to the wild-type with a 12374-, 21-, and 7530-fold increase in resistance,[2] respectively. This is a cause for worry, as the over 12000-fold reduction in efficacy shows that oseltamivir is not an effective treatment against the IRHY mutant strain.

The aim of this work was to investigate how the IR and IRHY mutations of H1N1-2009 NA lead to reduced binding efficacy of oseltamivir and zanamivir. To understand the mechanism of drug resistance, long time scale, explicit solvent MD simulations were performed using graphical processors (GPUs). In total, 1 $\mu$s of dynamics was performed, comprising ten 100 ns trajectories of the inhibitor bound and unbound forms of the wild-type protein and the IR and IRHY strains. The resulting trajectories were analyzed to investigate the effect of mutation and inhibitor binding on the conformation stability of the protein and, specifically, to understand, at a molecular level, why oseltamivir is no longer effective against the IRHY strain of H1N1-2009 NA.

## METHODS

**Preparing the Starting Structure.** The initial structure of H1N1-2009 NA was taken from the X-ray structure with protein data bank (PDB) code 3NSS.[13] Chain A of the dimer was used to provide the starting point for the simulation of the monomer wild-type unbound system (hereafter called WT). Simulation of the monomer was performed as simulations of the dimer would have been too computational demanding. To prepare the bound systems, oseltamivir and zanamivir coordinates were taken from PDB structures 2HU4[5] (oseltamivir bound to N1 from influenza-H5N1) and 1NNC[23] (zanamivir bound to N9 from influenza-H11N9), via superposition over the structure from 3NSS. Hydrogens were added to the inhibitors and the positions of these hydrogens optimized using Gaussian03[24] at the HF/6-31G* level of theory. This provided the starting point for the wild-type inhibitor-bound simulations, hereafter called WT:osel and WT:zana. For the mutant-strain simulations, the isoleucine (I) at position 223 was changed to an arginine (R), to create the single IR mutant (simulations hereafter called IR, IR:osel, and IR:zana), and residues I223 and H275 were changed to R223 and Y275 for the IRHY double mutant (simulations hereafter called IRHY, IRHY:osel, and IRHY:zana). All systems included the structurally important calcium ion,[25] with starting coordinates taken from 3NSS. All missing hydrogen atoms for each system were added using the LEaP module in AMBER 10.[26] The predicted ionization states for amino acid residues with potentially charged side chains were calculated using PROPKA.[27] All systems were solvated using TIP3P[28] water in an $\sim 90^3$ Å$^3$ box using $Cl^-$ as the


dx.doi.org/10.1021/bi300561n | Biochemistry 2012, 51, 4364−4375

neutralizing counterion. The generalized AMBER force field[29] (GAFF) was used to model the inhibitors, and the FF03[30] force field was used to model the protein. The atomic charges for the inhibitors were obtained using the RESP module implemented in AMBER 10,[26] based on an electrostatic potential calculated from a single point calculation at the HF/6-31G* level using Gaussian03.[24]

**Molecular Dynamics (MD) Simulations Using Graphical Processors (GPUs).** Energy minimization was used to optimize the positions of the hydrogen atoms and water molecules from each system using the SANDER module of AMBER 10.[26] This was followed by energy minimization of all atoms of each system. Molecular dynamics (MD) simulations were then performed using PMEMD.CUDA from AMBER 11.[31] PMEMD.CUDA is an experimental version of the PMEMD module that has been ported to run on graphical processors (GPUs) produced by nVidia. PMEMD.CUDA with bug fixes 1−11 (all bug fixes released up until 7/11/10) was used, with calculations performed on a cluster of nVidia Tesla C2050 GPU accelerators. Extensive testing was performed using this software/hardware combination on the NA system (WT:osel) to demonstrate that the results are comparable to those obtained using a CPU. Use of GPUs was chosen for this study because testing revealed that use of a GPU for this system was faster than using locally available CPUs (simulations using 1 GPU were ∼50% faster than those using 32 Xeon 3.4 GHz CPU cores). In addition, it was found that use of a GPU consumed significantly less energy (∼3 MJ per nanosecond of dynamics using 1 GPU compared to 10 MJ per nanosecond of using 32 CPU cores). Use of GPUs to run the 1 $\mu$s of dynamics required for this investigation therefore saved ∼7 GJ of electricity compared to running these calculations using locally available CPUs. GPUs provide promising systems for energy efficient scientific computing.

MD simulations were performed using a time step of 2 fs and a cutoff radius of 10 Å for the nonbonded interactions, and particle-mesh Ewald (PME) was used for calculating the long-range electrostatic interactions.[32] SHAKE[33] was used to constrain all bonds involving hydrogen. Initially, the temperature of each system was increased gradually from 0 to 310 K over a period of 100 ps of NVT dynamics. This was followed by 100 ps of NVT equilibration at 310 K and then 800 ps of NPT equilibration at 310 K and 1 atm pressure. The structures after this initial equilibration were checked visually for any problems. The resulting set of nine structures (WT, WT:osel, WT:zana, IR, IR:osel, IR:zana, IRHY, IRHY:osel, and IRHY:zana) were then used as input to nine 100 ns MD simulations. As the resistance of the IRHY mutant to oseltamivir was one of the key focuses of interest of this work, the IRHY:osel starting structure was duplicated and used as the starting point for a second 100 ns simulation (IRHY:osel2). A Langevin thermostat was used, with a random, random number seed given to each trajectory. It has been suggested that long time scale simulations of the monomer form of NA may be unstable.[15,34] This suggestion was based on observations of instability of the protein structure during implicit solvent (Generalized Born) MD simulations of the monomer. For example, the helix from D103-F115 was seen to unravel in simulations of the monomer but was stable during simulations of the tetramer.[15] This observation of instability of the monomer during an implicit solvent simulation led to the suggestion that explicit solvent simulations of the monomer should also use backbone restraints.[34] However, this suggestion was not tested in that study and does not appear to have been tested in any other work. As other workers have shown that short time scale (3 ns) explicit solvent MD simulations of N1 NA monomer without backbone restraints are stable,[11] it was decided that backbone restraints should not be used. As this study involved long time scale, unrestrained dynamics of the monomer, extra care was taken to monitor the stability of the simulations. The root-mean-square deviation (RMSD) of the trajectories was monitored, as was the root-mean-square fluctuations (RMSF), and the secondary structure assignment of each residue (see Supporting Information). These, together with visual inspection, showed that the dynamics of each trajectory was stable and that the helix from D103-F115 did not unravel. After ensuring stability, the first 20 ns of each of the ten resulting trajectories was discarded as equilibration, with analysis performed over only the final 80 ns. The full list of simulations performed is given in Table 1.

**Table 1. Naming Key for the Ten GPU Dynamics Simulations Performed for This Study**

| | wild-type | I223R mutant | I223R/H275Y mutant |
|---|---|---|---|
| unbound | WT | IR | IRHY |
| oseltamivir-bound | WT:osel | IR:osel | IRHY:osel, IRHY:osel2 |
| zanamivir-bound | WT:zana | IR:zana | IRHY:zana |

## RESULTS AND DISCUSSION

**Dynamics of the Free Protein.** All of the ten trajectories performed in this study were started from the closed form of H1N1-2009 NA, as taken from PDB structure 3NSS.[13] The first question to be asked by the study was whether the computer model was accurate and that a 100 ns trajectory was sufficient to observe the conformational change from the closed to the open form of the 150-loop. To answer this question, the three trajectories of the unbound protein were compared to crystal structures of the open and closed forms of NA. While, currently, no X-ray structure of the open form of H1N1-2009 is available, the structures of both the open and closed forms of the related N1 NA from the H5N1 "bird flu" influenza virus have been determined (2HU4 for closed[5] and 2HTY for open[5]). Snapshot structures from every 100 ps between 20 and 100 ns were sequence aligned and structurally aligned against both 2HU4 and 2HTY. The RMSD of the C$\alpha$-atoms of the residues in the 150-loop (residues 147 to 152) between each snapshot, and the aligned open and closed forms were calculated and are shown in Figure 1. Sequence and structural alignment was performed using the program CE.[35] Alignment was based on residues 130−146 and 153−170 to ensure that the effect of motion of the rest of the protein in the calculated RMSDs was minimized. Figure 2 shows the aligned structures of the WT trajectory, as compared to the open and closed forms of H5N1 NA. It is clear from these structures, and from the RMSDs in Figure 1a, that the 150-loop in the WT trajectory transitions slowly from the closed conformation at 20 ns to the open conformation at 100 ns. H1N1 NA differs from H5N1 NA as H1N1 NA has an isoleucine in the 150-loop (I149), while H5N1 NA has a valine (V149). During the trajectory, this structurally significant I149 residue is observed to rotate from a conformation that matches the experimentally observed V149 closed-loop conformation, to a conformation that matches the crystallographically observed V149 open-form conformation (see Figure 2). The observation of this transition in a free, unrestrained dynamics trajectory of the WT indicates that the conformational change from the closed to open form is being


dx.doi.org/10.1021/bi300561n | Biochemistry 2012, 51, 4364−4375

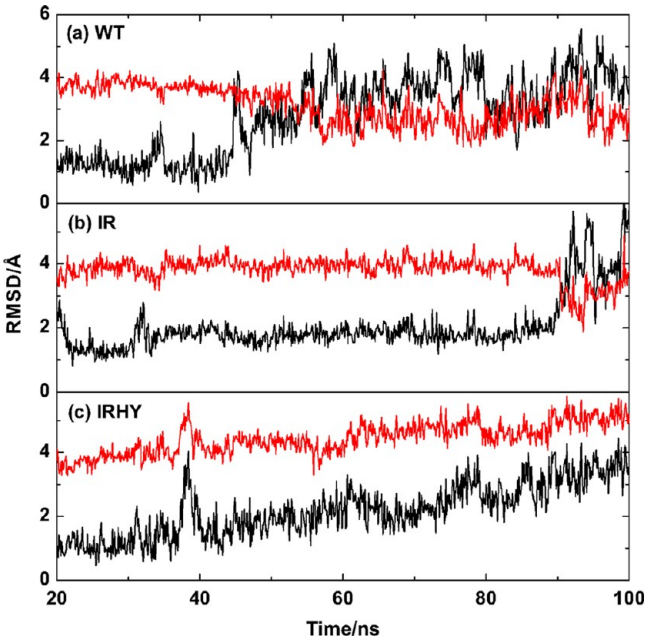


**Figure 1.** RMSDs of the Cα-atoms of the 150-loop for snapshots from the WT, IR, and IRHY free protein trajectories, as compared to the open (red) and closed (black) X-ray conformations of NA from H5N1.

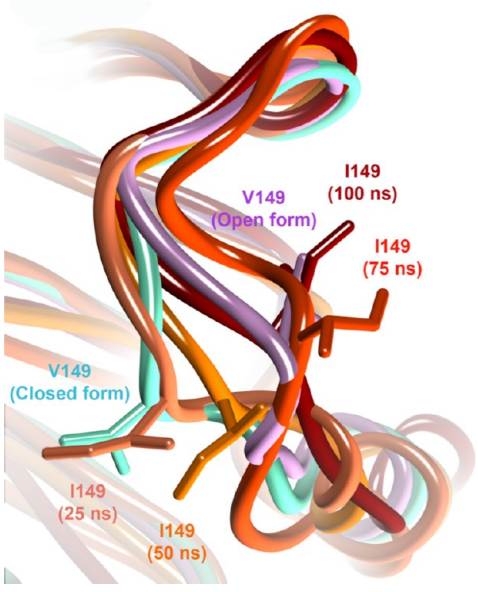


**Figure 2.** Structure of the 150-loop taken from the WT trajectory (shades of orange/red) compared with the 150-loop from the open (purple) and closed (cyan) X-ray conformations of NA from H5N1. The structurally significant V149 (H5N1)/I149 (H1N1) residue is shown, showing how, during the trajectory, it rotates from the closed-form orientation to the open-form orientation.

simulated correctly, thereby giving confidence in the underlying model. The simulation results also suggest that, while the apo form of H1N1-2009 was crystallized in the closed form, it is similar to other group 1 NAs and that the open form can be adopted and may be preferred in solution. These observations agree with those published recently by Amaro et al.,[16] who ran long time scale MD simulations of variants of NA that included H1N1-2009. In that work, similar conformational changes of the 150-loop were observed.

It is interesting to note that, while the transition from the closed to open forms occurs gradually during the trajectory for the WT, the closed form appears more stable in the IR mutant structure, with the transition occurring suddenly after about 90 ns of dynamics. At this point, the I149 residue quickly flips up from the closed to the open orientation over a time of about 5 ns. This shows that the orientation of the I149 residue is a good indicator of whether the 150-loop is open or closed. It is also worth noting that the 150-loop in the IRHY double mutant transitions does not change from the closed to the open conformation, and the I149 residue remains in the closed orientation. Instead, only the beginning of a possible conformational change is observed, with the RMSD against the closed form increasing after ∼70 ns, with no change in the RMSD against the open form, and no rotation of the I149 residue. The final structure of the trajectory is visually similar to the closed form, while for the WT and IR trajectories, the final structures are visually similar to the open form. This can be seen in Figure 3, in which the structures of the 150-loop at 20 and 100 ns are compared. This figure shows that the opening of 150-loop in the WT and IR trajectories was accompanied by an expansion of the 430-loop. A similar expansion of this loop was also observed during other computational studies.[14,15]

While 100 ns is long for an MD simulation, it is a short time on the biological time scale. The observation of conformational changes between the closed and open forms of the 150-loop in two out of the three trajectories suggests that the barrier to conformational change is low.

**Dynamics of the Bound Protein.** As simulations of free NA reveal conformational changes that map from the crystallographically known closed and open forms of the 150-loop, the next stage in the analysis was to determine whether similar conformational changes were observed in the simulations of the bound protein. The root-mean-square fluctuations (RMSF) of each residue from 20 to 100 ns was calculated and is shown in Figure 4, together with the aligned structures of the protein at 100 ns. These demonstrate clearly that the only trajectory to transition to the open conformation was IRHY:osel. This trajectory exhibits significantly more motion in the residues in the 150-loop region as compared to the other trajectories, and it is clear from the overlay of the final structure from dynamics that the final structure is open. As with the WT and IR simulations, the I149 residue has rotated during the IRHY:osel trajectory to match the conformation of the V149 residue in the open form H5N1 NA.

**Essential Dynamics of Loop Opening.** Principal components analysis (PCA[36]) was used to analyze the trajectories of the bound systems to see how point mutations and ligand binding affected the dynamics of NA. PCA was performed on the Cα-atoms of NA, using the Wordom structural analysis package.[37] The first two principal components of motion from each trajectory were calculated, and the full range of motion plotted. The IRHY:osel and WT:zana trajectories were the only ones for which the first two principal components of motion were focused on the 150-loop. These are shown in Figure 5 for the IRHY:osel trajectory. Movies along these two principal components are provided as Supporting Information, together with corresponding plots of the principal components for the other bound trajectories. These plots show that the 150-loop in the IRHY:osel and WT:zana trajectories was highly flexible. In the IRHY:osel trajectory, this flexibility corresponded to the loop opening event. In the WT:zana trajectory, no obvious loop opening event occurred, although the loop was more mobile, as is seen in the RMSFs in Figure 4b.


dx.doi.org/10.1021/bi300561n | Biochemistry 2012, 51, 4364−4375

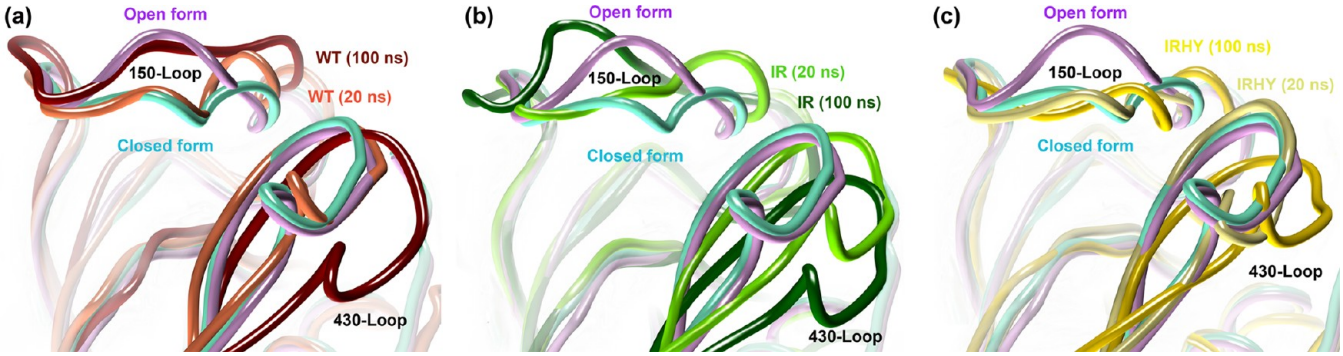


**Figure 3.** Structure of the 150-loop and 430-loop at 20 and 100 ns taken from the (a) WT, (b) IR, and (c) IRHY simulations, compared with the 150-loop and 430-loop from the open and closed X-ray conformations of NA from H5N1.

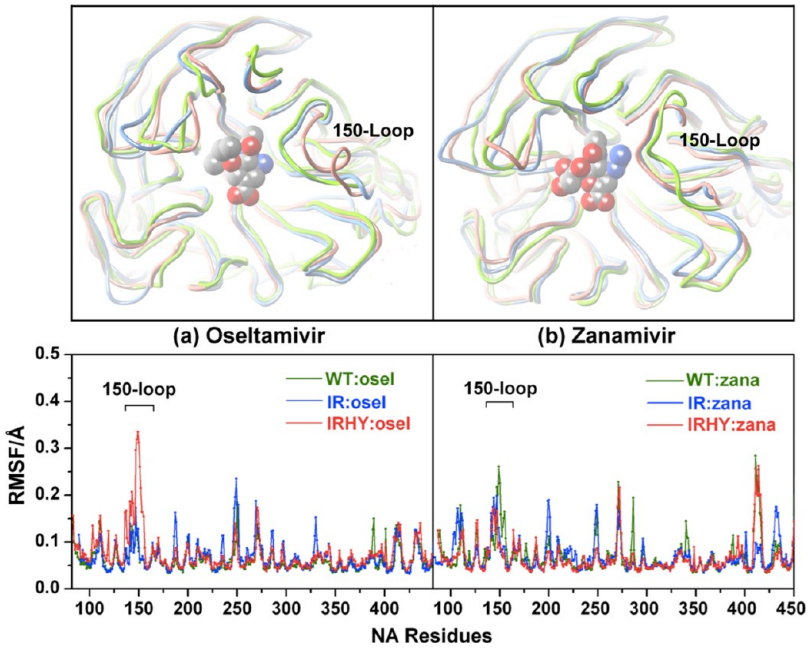


**Figure 4.** RMSFs of each residue from the inhibitor-bound simulations of NA for the wild-type (green) and IR (blue) and IRHY (red) mutants, together with a comparison of the backbone of the protein at the end of the 100 ns trajectory.

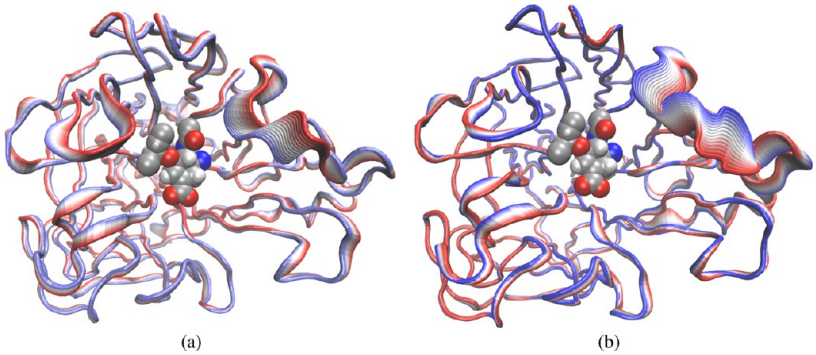


**Figure 5.** Structures representing the first (a) and second (b) most siginificant principal components of motion of the C$\alpha$-atoms of NA from the IRHY:osel trajectory, analyzed between 20 and 100 ns, colored showing the range of the principal component from red (maximum value) to blue (minimum value).

To investigate the rate of loop opening in IRHY:osel, each frame of the trajectory was projected back against the top two principal components (Figure 6). For comparison, similar projections are provided for the other bound trajectories in the Supporting Information. The projections for IRHY:osel reveal that the loop opening event, which is predominantly described by the first principal component, occurs over a time period of ~70 ns. After 70 ns, the trajectory jumps from a phase of gradual motion along the first principal component, to spend the remaining 30 ns of the trajectory oscillating around a constant value. In contrast, motion along the second principal component, which corresponds to a stretch/compress of the


dx.doi.org/10.1021/bi300561n | *Biochemistry* 2012, 51, 4364−4375

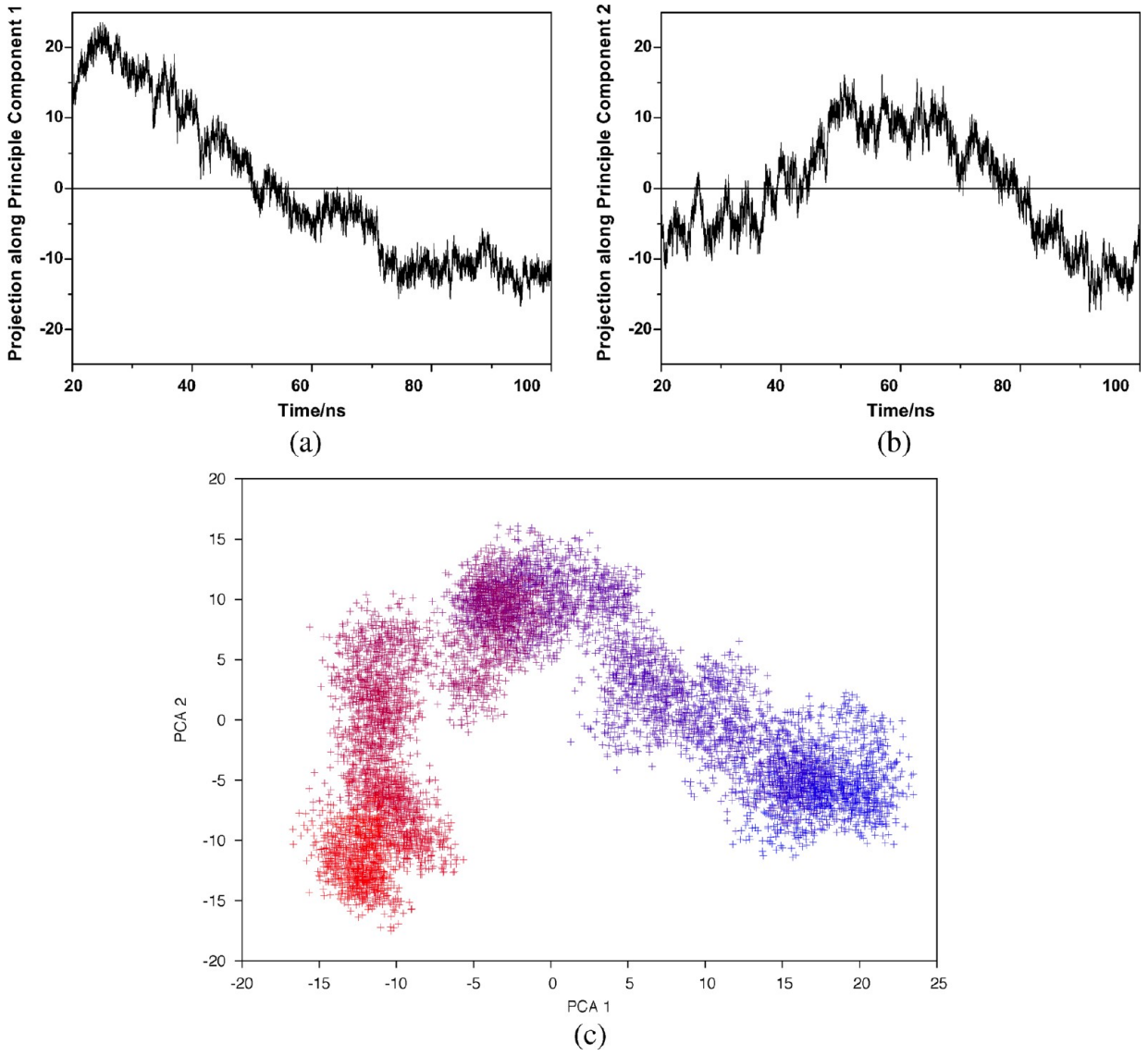


**Figure 6.** The projection along the first (a) and second (b) most significant principal components of motion of the C$\alpha$-atoms of NA from the IRHY:osel trajectory. The trajectory projected to the two-dimensional space described by these components is shown in (c), with a color scale used to indicate time (blue for the start of the trajectory at 20 ns and red for the end at 100 ns).

150-loop, occurs as a long time scale oscillation, with a period of ~65 ns.

This conformational change is observed only for the IRHY:osel trajectory. This confirms the observation from the RMSF analysis that, with the exception of IRHY:osel, the closed conformation of the 150-loop for the inhibitor bound structures is stable over the lifetime of the MD trajectories.

**Mechanism of Loop Opening.** It is clear from analysis of the trajectories that, while the open form of NA is preferred for the WT and IR free proteins, binding of inhibitors to the wild-type or mutants resulted in a closed form structure that was stable, at least for the 100 ns duration of the simulation. The only exception was IRHY:osel, which showed a marked conformational change in the 150-loop to the open form. To investigate why this was the case, distances between the NA inhibitors and key residues and between key residues in the active site were calculated and are shown in Figure 7. To avoid artifacts caused by hydrogen bonds (H-bonds) switching between equivalent atoms, each distance was measured by calculating the distance between all equivalent atom pairs for each frame of the trajectory and then selecting the smallest value. The Wordom[37] structural analysis package was used to calculate distances, and the atom pairs used are described in Table 2 and shown in Figure 7. These atoms pairs were chosen as they (mostly) corresponded to key hydrogen bond interactions in the wild-type or mutant structures.

H-bonds are typified by interatomic distances that are less than 3.5 Å, and so H-bonds show up as blue and blue/green regions in Figure 7. This figure shows that both oseltamivir and zanamivir are able to make hydrogen bonds with the D151 and R152 residues of the 150-loop. However, it also shows that there is competition between R223 and R152 in the IR and IRHY mutants. Both IR and IRHY involve a mutation of the isoleucine (I223) to an arginine (R223). In the wild-type, I223 is a hydrophobic framework residue that stabilizes the NA active site by interacting with the hydrophobic R-group of the NA inhibitors.[8] In the mutants, R223 is a charged residue, with Figure 7 showing competition with R152 from the 150-loop for the H-bond to the *N*-acetyl group of the inhibitors.


dx.doi.org/10.1021/bi300561n | *Biochemistry* 2012, 51, 4364−4375

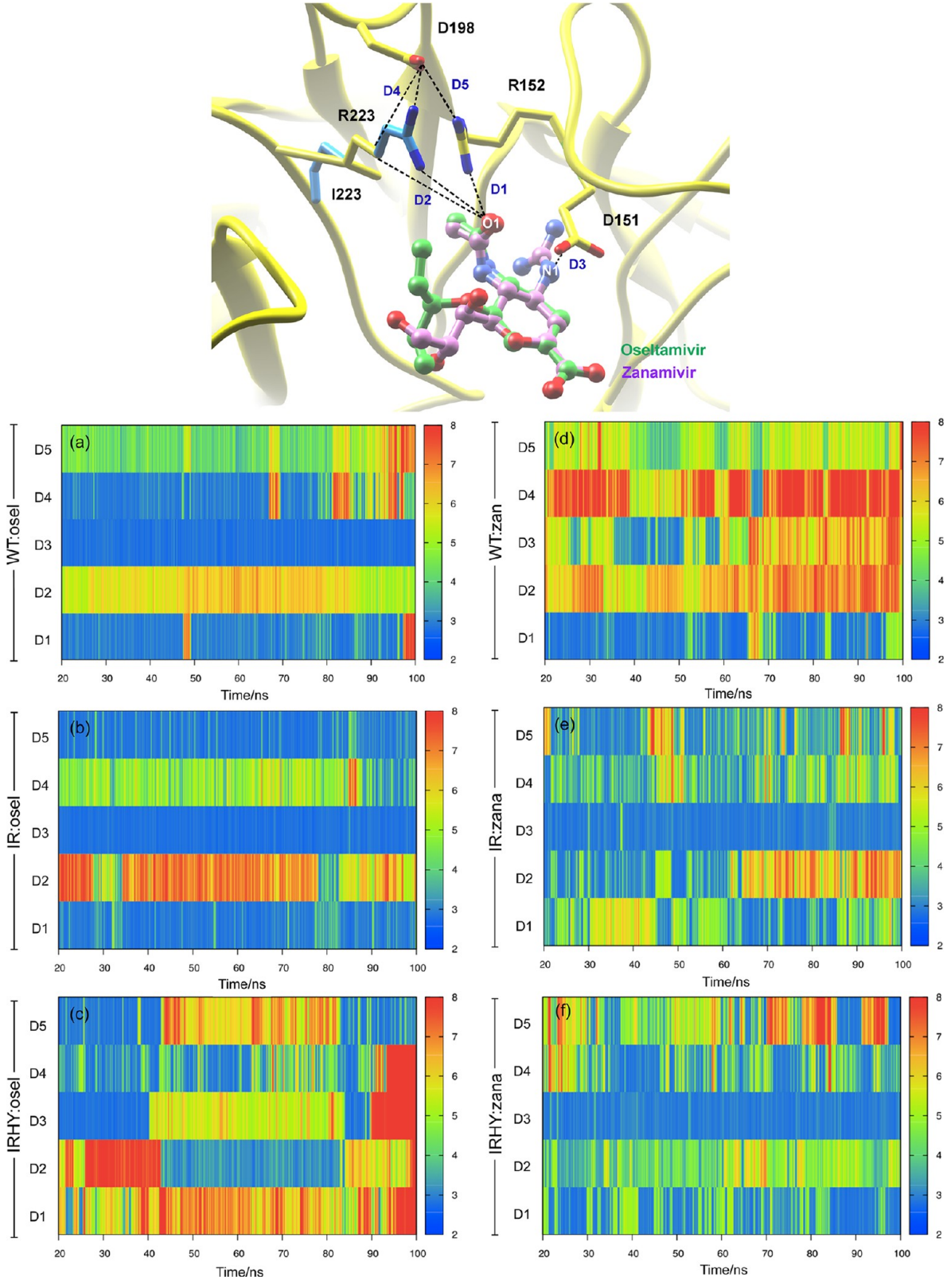


**Figure 7.** Values of distances that represent key interactions in the active site of NA. The distances D1−D5 are calculated between atoms as indicated in the schematic at the top and described in Table 2. The distances are plotted on a color scale from blue (less than or equal to 2 Å) to red (greater than or equal to 8 Å).

For oseltamivir in WT:osel and IR:osel, the H-bond to D151 (D3) is strong and maintained throughout the trajectory. The H-bond to R152 (D1) is still strong but breaks for short time periods periodically, breaking more in the IR:osel trajectory due to competition from R223. Competition between R152 and R223 for the H-bond to oseltamivir is more intense in the IRHY:osel trajectory, and both residues compete such that neither are H-bonding to the inhibitor at 20 ns. The H-bond


dx.doi.org/10.1021/bi300561n | *Biochemistry* 2012, 51, 4364−4375

**Table 2. Five Sets of Atom Pairs Used To Calculate the Distances That Are Analyzed in Figures 7 and 8**

| distance | protein atoms | selected atoms |
|---|---|---|
| D1 | R152: NH1 or NH2 | osel: O1, zana: O1 |
| D2 | I223: CD1, R223: NH1 or NH2 | osel: O1, zana: O1 |
| D3 | D151: OD1 or OD2 | osel: N1, zana: N1 |
| D4 | D198: OD1 or OD2 | I223: CD1, R223: NH1 or NH2 |
| D5 | D198: OD1 or OD2 | R152: NH1 or NH2 |

between oseltamivir and D151 (D3) is broken at ∼40 ns, thereby allowing R223 to pull the inhibitor closer and form a H-bond (D2). This means that there are then no H-bonds between oseltamivir and the 150-loop, thereby releasing the 150-loop and allowing it to transition into the open conformation. PCA analysis presented in the last section showed that this conformational change took until about 70 ns. While this is not clear from the distance plot, it is clear that after 80 ns, once the 150-loop is fully open, the H-bond between oseltamivir and the mutant R223 residue is broken. The inhibitor then briefly H-bonds to the D151 residue on the 150-loop, before it begins to be expelled from the active site. A movie showing the conformational change of the 150-loop and the beginning of oseltamivir being expelled from the active site is available in the Supporting Information.

The binding efficacy of zanamivir is affected less by the IR and IRHY mutations as it is able to maintain H-bonding to the 150-loop. This is despite competition from the mutant R223 residue. In the WT, it is the H-bond between zanamivir and the R152 residue (D1) that is strong, while the H-bond to D151 (D3) is weak and transient (and indeed breaks by the end of the WT:zana trajectory). This is the opposite of the WT:osel trajectory and may account for the increased flexibility of the 150-loop seen in WT:zana in the RMSF and PCA analysis. In the IR:zana and IRHY:zana trajectories, competition from the R223 residue weakens the R152 H-bond, but zanamivir compensates by strengthening the H-bond to D151, thereby locking the 150-loop in place. It is able to do this as it H-bonds to D151 using a large, positively charged guanadinium group, as compared to oseltamivir that uses a smaller $-NH_3^+$ group. Zanamivir is sufficiently large to be able to bridge between the D151 residue and mutant R223 residue. Oseltamivir cannot bridge, so it is forced to choose to H-bond to one or the other of these residues. Oseltamivir swapping from D151 to R223 frees the 150-loop to transition into the open conformation.

While these simulations are long on the MD time scale, they are short on the biological time scale. These results demonstrate only that the change from the closed to open conformation of the 150-loop can occur while the IRHY NA mutant is bound to oseltamivir and provide one mechanism for the opening that takes place over a time period of ∼70 ns. To gain more confidence in the results, the second IRHY:osel trajectory (IRHY:osel2) was analyzed. The analysis showed that, while the trajectory showed many similarities to the beginning of the IRHY:osel trajectory, a loop opening event had not occurred. The distances of key atom pairs for the IRHY:osel2 trajectory, placed next to those from the IRHY:osel trajectory, is shown in Figure 8. This shows the same competition between the R152 and R223 residues for H-bonding to oseltamivir, with this competition leading to the breaking of the H-bonds to both residues after 80 ns. This is the first step of the mechanism of loop opening that was observed in the IRHY:osel trajectory, and it is interesting to note that the H-bonding pattern in IRHY:osel2 at 100 ns is similar to that in IRHY:osel at 20 ns. This suggests that the loop opening mechanism is triggered by two rare events; first the breaking of the R152 H-bond, which was immediate in IRHY:osel, but which did not occur until after 80 ns in IRHY:osel2, and second, the breaking of the D151 H-bond, which occurred at least 40 ns after the breaking of the R152 H-bond in the IRHY:osel trajectory and had not yet occurred by the end of the 100 ns IRHY:osel2 trajectory. To confirm these observations, more dynamics simulations would need to be performed, including both further repeats of the IRHY:osel trajectory and extensions of these trajectories to at least 200 ns. In addition, while loop opening events were not observed in any of the zanamivir-bound trajectories, or for the oseltamivir-bound WT or IR trajectories, it is possible that this was because, by chance, the rare event of breaking the R152 H-bond had not occurred. Again, more dynamics simulations of these systems are necessary, although this requires computational resources that were beyond what was available for this study, but that should be the subject of future work. All simulation output files and input files can be downloaded by getting in contact with the authors, and these can be used to continue, expand, or repeat this study.

Despite the need for more simulations, the trajectories show good agreement with experiment and provide a plausible molecular mechanism for the emergence of strains of influenza that are resistant to oseltamivir. The results suggests that the double mutation (I223R/H275Y) causes a high level of resistance due to the loss of hydrogen bonds between the inhibitor and key residues in the 150-loop (D151 and R152). The mutation at

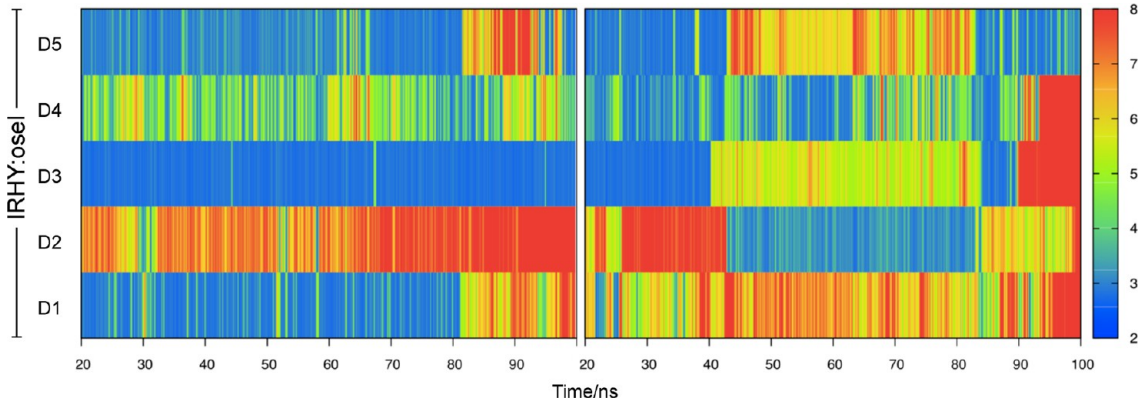


**Figure 8.** Distances of key interacting atom pairs from the IRHY:osel2 trajectory (left) as compared to those from the IRHY:osel trajectory (right). The atom pairs used to calculate distances are described in Table 2 and shown in Figure 7.


dx.doi.org/10.1021/bi300561n | *Biochemistry* 2012, 51, 4364−4375

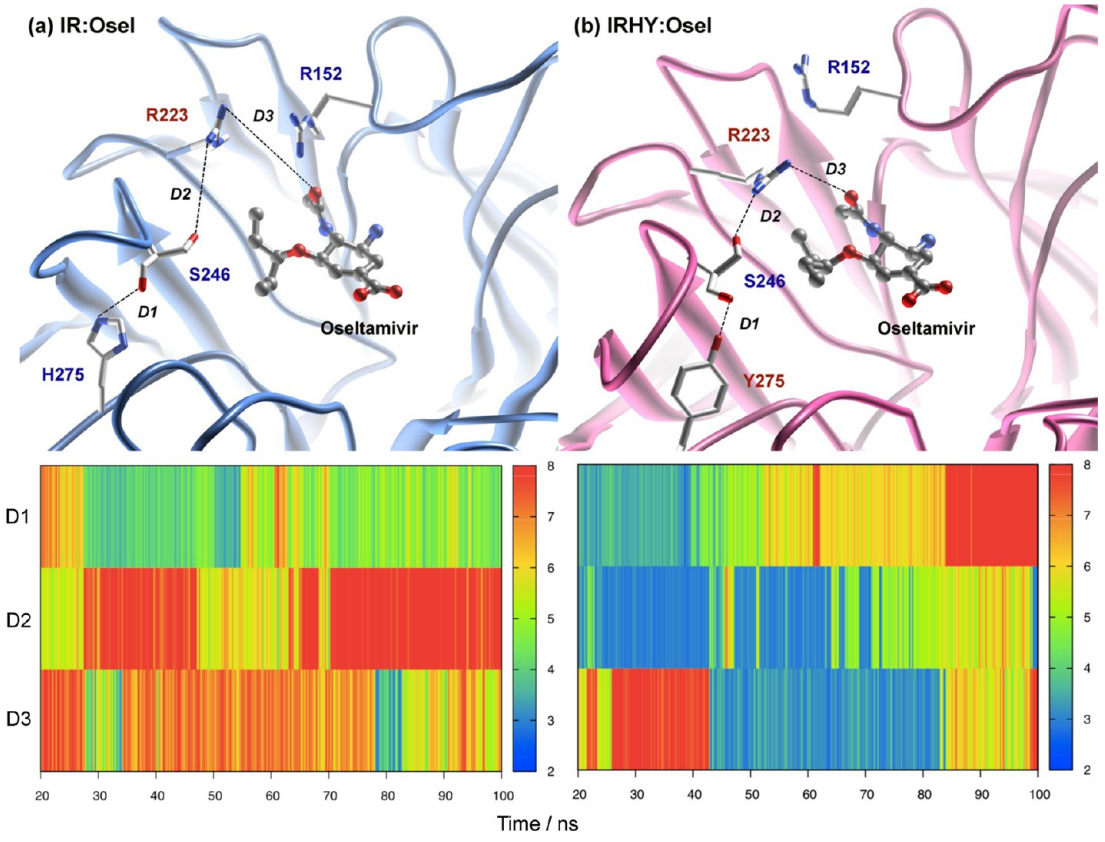


**Figure 9.** Distances between key atom pairs representing hydrogen bonding demonstrating the role of S246 as a briding residue between the two mutant residues (I223R and H275Y) and oseltamivir in the IR:osel and IRHY:osel trajectories.

I223R reduces binding efficacy by competing with R152 for a hydrogen bond to the *N*-acetyl group of the inhibitors. Zanamivir binding is maintained, as on the loss of this H-bond, zanamivir switched to H-bond strongly to the D151 residue in the 150 loop. Zanamivir was capable of making a strong H-bond because of it having a larger guanidinium group. Oseltamivir has a small amino group and so could not stretch to make a strong H-bond with D151. In the IRHY mutant, forming the H-bond to R223 pulled oseltamivir away from the 150-loop, thereby freeing the loop to change into the open conformation. This mechanism suggests drug resistance could be overcome either by increasing the strength of hydrogen bond interactions between the ligand and the D151 and R152 residues in the 150-loop, so as to pin shut the closed conformation, or that the ligand should be designed to be able to make an additional H-bond to the R223 mutant residue, thereby preventing competition between R223 and R152.

**Role of the H275Y Mutation.** The results presented provide a clear molecular mechanism for oseltamivir resistance in the double IRHY mutant. Oseltamivir resistance has also been previously observed in N1 NA in the single H275Y ("HY") mutant.[18,19] Several X-ray crystallography and molecular modeling studies have investigated the mechanism of drug resistance in the HY mutant.[38−41] The hydrophobic R group of oseltamivir binds into a hydrophobic pocket formed by residues R224 and E276 that lie next to H275Y.[39] Tyrosine is larger than histidine, so it has been suggested that the HY mutation reduces the size of the hydrophobic pocket and that this leads to high resistance to oseltamivir.[40]

In this work, the IRHY mutant is indicated to be resistant, not because of the direct effect of the HY mutation but because of competition between the R223 mutant residue and R152 on the 150-loop. This leads to the questions of the role of the HY mutation and to why the competition between R223 and R152 is less pronounced in the single IR mutant. The answers were provided by a visual examination of the trajectories. This showed that residue S246 acted as a bridge between the HY and IR mutant residues, as can be seen in Figure 9.

In the IRHY:osel trajectory, the hydroxyl group of the mutant Y275 was found to form a H-bond with the backbone carbonyl group of S246 (distance D1). This stabilized the H-bond interaction between S246 and R223 (D2). This kept R223 pointing into the binding site in a conformation that allowed it to compete with R152 for the H-bond to oseltamivir (D3). The H275 residue is too small to H-bond with S246, and this H-bond was not seen in the IR:osel trajectory. There are almost no H-bonds during the trajectory for the IR mutant in Figure 9, while for IRHY:osel, residues Y275, S246, and R223 form a H-bond network at the beginning of the trajectory (distances D1 and D2). This allowed R223 to maintain a conformation that enabled it to compete with R152 and then H-bond with oseltamivir at about 40 ns. This led to the breaking of the H-bond between Y275 and S246 (D1), with S246 then stabilizing R223 (D3) as it H-bonds with oseltamivir. This holds the H-bond in place for sufficiently long for the 150-loop to open at 70 ns, until all the H-bonds break at about 80 ns when the 150-loop has opened completely due to the loss of H-bonds between oseltamivir and R152 and D151. S246 is thus a key residue in the mechanism for resistance, as it links the two mutant residues in IRHY. The importantance of S246 has been confirmed by the appearance recently of novel S246N mutant strains of N1 NA.[42] These mutants show reduced oseltamivir


dx.doi.org/10.1021/bi300561n | *Biochemistry* 2012, 51, 4364−4375

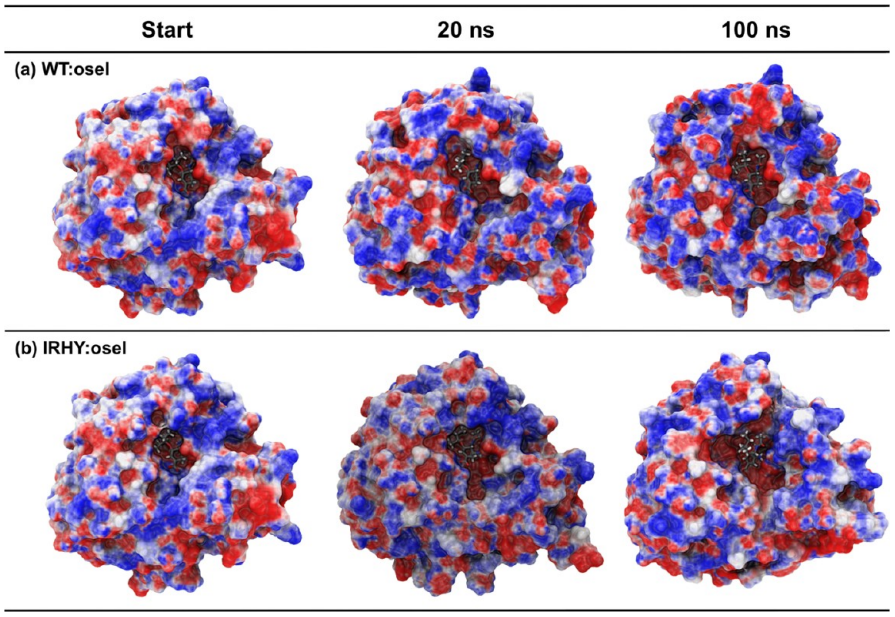


**Figure 10.** Electrostatic potential on the surface of NA for the starting structure, and 20 and 100 ns snapshots taken from the WT:osel and IRHY:osel trajectories. Regions of negative electrostatic potential are shown in red, positive in blue, and neutral in white.

efficacy and appeared while the work presented here was in progress between January and March 2011.[42]

**Electrostatic Consequences of the Closed and Open Conformations.** Long time scale MD simulations have shown that the 150-loop of the IRHY double mutant can undergo conformational change from the closed to open form while bound to oseltamivir. X-ray[5] and computational[11] studies suggest that oseltamivir binds poorly to the open conformation. To investigate why this is the case, Poisson−Boltzmann electrostatic calculations were performed for snapshots of NA taken from the WT:osel and IRHY:osel trajectories. The coordinates of the protein atoms were taken from the starting structure, and from snapshots taken after 20 and 100 ns of simulation. The electrostatic potential on the surface of the protein was calculated using APBS,[43] via the APBS electrostatics extension to VMD 1.8.7.[44] Default options were used to calculate the electrostatic potential over the entire protein surface, using a protein dielectric of 1.0, solvent dielectric of 78.54, a 129 × 129 × 129 grid, using a solvent radius of 1.4 Å. Charges were assigned from the FF99 force field using PDB2PQR.[45]

The resulting electrostatic potential on the surface of NA is shown in Figure 10. This shows that oseltamivir shows good shape and electrostatic complementarity to the closed conformation of WT NA. This is unsurprising, as this inhibitor was designed to target the closed conformation of group 2 NA. Oseltamivir fits tightly into the cavity of the active site, with its negatively charged carboxylate group sitting in a region of positive electrostatic potential, while the positively charged amino group sits deep in a negative potential pocket. This electrostatic complementarity is maintained during the entire 100 ns WT:osel trajectory, even as a small cavity opens next to the inhibitor.

While oseltamivir shows good shape and electrostatic complementarity to the closed form of NA that exists at 20 ns in IRHY:osel, this is lost during the subsequent steps of the trajectory. The conformational changes associated with the transition to the open form of the 150-loop lead to the opening of large cavities all around the inhibitor. This opens up a large, negative potential cavity, to which oseltamivir is no longer suited. It is unsurprising that oseltamivir binds poorly to this large, negative cavity, as its negatively charged carboxylate group is now in a region of negative electrostatic potential, and the opening of the 150-loop exposes the positive amino group of oseltamivir to solvent. The conclusion from these APBS calculations is supported by the observation that oseltamivir begins to unbind from NA at the end of the IRHY:osel trajectory. Support is also provided by previous MM/PBSA calculations on the related H5N1 NA,[11] which show that the absolute binding free energy of oseltamivir to the open form was +12.4 kcal mol$^{-1}$, compared to −8.5 kcal mol$^{-1}$ for the closed form. It would be useful to confirm these values by using the open and closed structures of the complexes generated from this study as starting points for more sophisticated, explicit solvent absolute binding free energy calculations.[46]

## CONCLUSION

The effect of point mutations on the dynamics of NA from H1N1-2009 influenza was studied using long time scale molecular dynamics simulations. The aim was to investigate why oseltamivir (Tamiflu) is ineffective as a treatment against the double mutant IRHY of NA. The wild-type, IR, and IRHY mutants were investigated, both in the free form and complexed with oseltamivir and zanamivir. The results demonstrated that, while the 150-loop of the unbound protein adopted an open structure for wild-type and IR NA, the presence of the inhibitors stabilized the closed conformation, at least over the 100 ns time scale of the simulation. The exception was the double mutant, IRHY, when bound to oseltamivir. Conformational change from the closed to open form of the 150-loop of the double mutant was observed over a period of 70 ns while bound to oseltamivir. This suggests that the double mutation causes a high level of resistance due to the loss of hydrogen bonds between the inhibitor and key residues in the 150-loop (D151 and R152). The mutation at I223R reduces binding efficacy by competing with R152 for a hydrogen bond to the *N*-acetyl group of the inhibitors. Zanamivir binding is maintained, as on the loss of this H-bond, zanamivir switched to


dx.doi.org/10.1021/bi300561n | *Biochemistry* 2012, 51, 4364−4375

H-bond strongly to the D151 residue in the 150 loop. Zanamivir was capable of making a strong H-bond because of it having a larger guanidinium group. Oseltamivir has a small amino group and so could not stretch to make a strong H-bond with D151. In the IRHY mutant, forming the H-bond to R223 pulled oseltamivir away from the 150-loop, breaking the H-bond with D151, thereby freeing the 150-loop to change into the open conformation. Electrostatic analysis confirms the experimental observation and other computational studies that oseltamivir is not matched to the open form, and it thus does not bind. These results agree with experiment and provide a plausible molecular mechanism for the emergence of strains of influenza virus that are resistant to oseltamivir. This mechanism suggests drug resistance could be overcome either by increasing the strength of hydrogen bond interactions between the ligand and the D151 and R152 residues in the 150-loop, so as to pin shut the closed conformation, or that the ligand should be designed to be able to make an additional H-bond to the R223 mutant residue, thereby preventing competition between R223 and R152.

## ■ ASSOCIATED CONTENT

### Supporting Information

RMSDs (Figure Supp1) and secondary structure assignments (Figure Supp2) for of all of the trajectories, a movie of the IRHY:osel trajectory, showing the loop opening, and beginning of the ligand unbinding events, a movie of the first and second principal components of motion of the IRHY:osel trajectory, figures showing the first and second principal components of motion for the other bound trajectories (Figures Supp3 and Supp4, equivalent to Figure 5), and the projection of those trajectories along the first and second principal components (Figure Supp5, equivalent to Figure 6c). This material is available free of charge via the Internet at http://pubs.acs.org.

## ■ AUTHOR INFORMATION

### Corresponding Author

*E-mail Christopher.Woods@bristol.ac.uk (C.J.W.), Adrian.Mulholland@bristol.ac.uk (A.J.M.); Ph +44-(0)117-928-9097; Fax +44-(0)117-9277985.

### Funding

The authors thank the Chulalongkorn University Centenary Academic Development and The Higher Education Research Promotion and National Research University Project of Thailand, Office of the Higher Education Commission (HR1155A) and The Thai Government Stimulus Package 2, and the EPSRC (EP/I030395/1) for funding this work. A.J.M. is an EPSRC Leadership Fellow EP/G007705/1.

### Notes

The authors declare no competing financial interest.

## ■ ACKNOWLEDGMENTS

The work was carried out with the kind support and the computational facilities of the University of Bristol Advanced Computing Research Center. The authors gratefully thank Dr. M. van der Kamp and Dr. J. McGeagh for useful discussions on the subject of protein structural analysis.

## ■ REFERENCES

(1) van der Vries, E., Stelma, F. F., and Boucher, C. A. (2010) Emergence of a multidrug-resistant pandemic influenza A (H1N1) virus. *N. Engl. J. Med. 363*, 1381−1382.

(2) Nguyen, H. T., Fry, A. M., Loveless, P. A., Klimov, A. I., and Gubareva, L. V. (2010) Recovery of a multidrug-resistant strain of pandemic influenza A 2009 (H1N1) virus carrying a dual H275Y/I223R mutation from a child after prolonged treatment with oseltamivir. *Clin. Infect. Dis. 51*, 983−984.

(3) Swerdlow, D. L., Finelli, L., and Bridges, C. B. (2011) 2009 H1N1 influenza pandemic: field and epidemiologic investigations in the United States at the start of the first pandemic of the 21st century. *Clin. Infect. Dis. 52* (Suppl1), S1−3.

(4) Al-Muharrmi, Z. (2010) Understanding the influenza A H1N1 2009 pandemic. *Sultan. Qaboos. Univ. Med. J. 10*, 187−195.

(5) Russell, R. J., Haire, L. F., Stevens, D. J., Collins, P. J., Lin, Y. P., Blackburn, G. M., Hay, A. J., Gamblin, S. J., and Skehel, J. J. (2006) The structure of H5N1 avian influenza neuraminidase suggests new opportunities for drug design. *Nature 443*, 45−49.

(6) Kim, C. U., Lew, W., Williams, M. A., Liu, H., Zhang, L., Swaminathan, S., Bischofberger, N., Chen, M. S., Mendel, D. B., Tai, C. Y., Laver, W. G., and Stevens, R. C. (1997) Influenza neuraminidase inhibitors possessing a novel hydrophobic interaction in the enzyme active site: design, synthesis, and structural analysis of carbocyclic sialic acid analogues with potent anti-influenza activity. *J. Am. Chem. Soc. 119*, 681−690.

(7) von Itzstein, M., et al. (1993) Rational design of potent sialidase-based inhibitors of influenza virus replication. *Nature 363*, 418−423.

(8) De Clercq, E. D. (2006) Antiviral agents active against influenza A viruses. *Nat. Rev. Drug Discovery 5*, 1015−1025.

(9) Xu, X., Zhu, X., Dwek, R. A., Stevens, J., and Wilson, I. A. (2008) Structural characterization of the 1918 influenza virus H1N1 neuraminidase. *J. Virol. 82*, 10493−10501.

(10) Wang, M., Qi, J., Liu, Y., Vavricka, C. J., Wu, Y., Li, Q., and Gao, G. F. (2011) Influenza A virus N5 neuraminidase has an extended 150-cavity. *J. Virol. 85*, 8431−8535.

(11) Wang, P., and Zhang, J. Z. H. (2010) Selective binding of anti influenza drugs and their analogues to "Open" and "Closed" conformations of H5N1 neuraminidase. *J. Phys. Chem. B 114*, 12958−12964.

(12) Xu, R., Ekiert, D. C., Krause, J. C., Hai, R., Crowe, J. E., Jr., and Wilson, I. A. (2010) Structural basis of preexisting immunity to the 2009 H1N1 pandemic influenza virus. *Science 328*, 357−360.

(13) Li, Q., et al. (2010) The 2009 pandemic H1N1 neuraminidase N1 lacks the 150-cavity in its active site. *Nat. Struct. Mol. Biol. 17*, 1266−1268.

(14) Amaro, R. E., Minh, D. D. L., Cheng, L. S., Lindstrom, W. M., Jr., Olson, A. J., Lin, J.-H., Li, W. W., and McCammon, J. A. (2007) Remarkable loop flexibility in avian influenza N1 and its implications for antiviral drug design. *J. Am. Chem. Soc. 129*, 7764−7765.

(15) Amaro, R. E., Cheng, X., Ivanov, I., Xu, D., and McCammon, J. A. (2009) Characterizing loop dynamics and ligand recognition in human- and avian-type influenza neuraminidases via Generalized Born molecular dynamics and end-point free energy calculations. *J. Am. Chem. Soc. 131*, 4702−4709.

(16) Amaro, R. E., Swift, R. V., Votapka, L., Li, W. W., Walker, R. C., and Bush, R. M. (2011) Mechanism of 150-cavity formation in influenza neuraminidase. *Nat. Commun. 12*, 388.

(17) Influenza (Flu) antiviral drugs and related information. Available from: http://www.fda.gov/Drugs/DrugSafety/InformationbyDrugClass/ucm100228.htm, Sept 2010.

(18) Ferraris, O., and Lina, B. (2008) Mutations of neuraminidase implicated in neuraminidase inhibitors resistance. *J. Clin. Virol. 41*, 13−19.

(19) Reece, P. A. (2007) Neuraminidase inhibitor resistance in influenza viruses. *J. Med. Virol. 79*, 1577−1586.

(20) Weekly update on oseltamivir resistance to pandemic influenza A (H1N1) 2009 viruses. Geneva: World Health Organization, 2010. (http://www.who.int/csr/disease/influenza/2011_05_06_weekly_web_update_oseltamivir_resistance.pdf), 2010.

(21) Eshaghi, A., Patel, S. N., Sarabia, A., Higgins, R. R., Savchenko, A., Stojios, P. J., Li, Y., Bastien, N., Alexander, D. C., Low, D. E., and

Gubbay, J. B. (2011) Multidrug-resistant pandemic (H1N1) 2009 infection in immunocompetent child. *Emerging Infect. Dis. 17*, xxxx.
(22) van der Vries, E., Kroeze, E. J. V., Stittelaar, K. J., Linster, M., der Linden, A. V., Schrauwen, E. J. A., Leijten, L. M., van Amerongen, G., Schutten, M., Kuiken, T., Osterhaus, A. D. M. E., Fouchier, R. A. M., Boucher, C. A. B., and Herfst, S. (2011) Multidrug resistant 2009 A/H1N1 influenza clinical isolate with a neuraminidase I223R mutation retains its virulence and transmissibility in ferrets. *PLoS Pathog. 7*, e1002276.
(23) Varghese, J. N., Epa, V. C., and Colman, P. M. (1995) Three-dimensional structure of the complex of 4-guanidino-Neu5Ac2en and influenza virus neuraminidase. *Protein Sci. 4*, 1081−1087.
(24) Frisch, M. J., et al. (2004) *Gaussian 03, Revision C.02*, Gaussian, Inc., Wallingford, CT.
(25) Lawrenz, M., Wereszczynski, J., Amaro, R., Walker, R. C., Roitberg, A. E., and McCammon, J. A. (2010) Impact of calcium on N1 influenza neuraminidase dynamics and binding free energy. *Proteins 78*, 2523−2532.
(26) Case, D., et al. (2008) AMBER 10. 2008, University of California, San Francisco.
(27) Li, H., Robertson, A. D., and Jensen, J. H. (2005) Very fast empirical prediction and rationalization of protein pKa values. *Proteins 61*, 704−721.
(28) Jorgensen, W. L., Chandrasekhar, J., Madura, J. D., Impey, R. W., and Klein, M. L. (1983) Comparison of simple potential functions for simulating liquid water. *J. Chem. Phys. 79*, 926−935.
(29) Wang, J., Wolf, R. M., Caldwell, J. W., Kollman, P. A., and Case, D. A. (2004) Development and testing of a general AMBER force field. *J. Comput. Chem. 25*, 1157−1174.
(30) Duan, Y., Wu, C., Chowdhury, S., Lee, M. C., Xiong, G., Zhang, W., Yang, R., Cieplak, P., Luo, R., Lee, T., Caldwell, J., Wang, J., and Kollman, P. (2003) A point-charge force field for molecular mechanics simulations of proteins based on condensed-phase quantum mechanical calculations. *J. Comput. Chem.*, 1999−2012.
(31) Case, D., et al. (2010) *AMBER 11*, University of California, San Francisco.
(32) Cornell, W. D., Cieplak, P., Bayly, C. I., Gould, I. R., Merz, K. M., Ferguson, D. M., Spellmeyer, D. C., Fox, T., Caldwell, J. W., and Kollman, P. A. (1995) A second generation force field for the simulation of proteins, nucleic acids, and organic molecules. *J. Am. Chem. Soc. 117*, 5179−5197.
(33) Ryckaert, J. P., Ciccotti, G., and Berendsen, H. J. C. (1997) Numerical integration of the cartesian equations of motion of a system with constraints: molecular dynamics of n-alkanes. *J. Comput. Phys.*, 327−341.
(34) Chachra, R., and Rizzo, R. C. (2008) Origins of resistance conferred by the R292K neuraminidase mutation via molecular dynamics and free energy calculations. *J. Chem. Theory Comput. 4*, 1526−1540.
(35) Shindyalov, I. N., and Bourne, P. E. (1998) Protein structure alignment by incremental combinatorial extension (CE) of the optimal path. *Protein Eng. 11*, 739−747.
(36) Amadei, A., Linssen, A. B., and Berendsen, H. J. (1993) Essential dynamics of proteins. *Proteins 17*, 412−425.
(37) Seeber, M., Cecchini, M., Rao, F., Settanni, G., and Caflisch, A. (2007) Wordom: a program for efficient analysis of molecular dynamics simulations. *Bioinformatics 23*, 2625−2627.
(38) Collins, P. J., Haire, L. F., Lin, Y. P., Liu, J., Russell, R. J., Walker, P. A., Skehel, J. J., Martin, S. R., Hay, A. J., and Gamblin, S. J. (2008) Crystal structures of oseltamivir-resistant influenza virus neuraminidase mutants. *Nature 453*, 1258−1261.
(39) Moscona, A. (2005) Oseltamivir resistance−disabling our influenza defenses. *N. Engl. J. Med. 353*, 2633−2636.
(40) Malaisree, M., Rungrotmongkol, T., Nunthaboot, N., Aruksakunwong, O., Intharathep, P., Decha, P., Sompornpisut, P., and Hannongbua, S. (2009) Source of oseltamivir resistance in avian influenza H5N1 virus with the H274Y mutation. *Amino Acids 37*, 725−732.
(41) Le, L., Lee, E. H., Hardy, D. J., Truong, T. N., and Schulten, K. (2010) Molecular dynamics simulations suggest that electrostatic funnel directs binding of tamiflu to influenza N1 neuraminidases. *PLoS Comput. Biol. 6*, e1000939.
(42) Hurt, A. C., Lee, R. T., Leang, S. K., Cui, L., Deng, Y. M., Phuah, S. P., Caldwell, N., Freeman, K., Komadina, N., Smith, D., Speers, D., Kelso, A., Lin, R. T., Maurer-Stroh, S., Barr, I. G. (2011) Increased detection in Australia and Singapore of a novel influenza A(H1N1)-2009 variant with reduced oseltamivir and zanamivir sensitivity due to a S247N neuraminidase mutation. *Euro Surveill. 16*, 19884, Available online: http://www.eurosurveillance.org/ViewArticle.aspx?ArticleId=19884.
(43) Baker, N. A., Sept, D., Joseph, S., Holst, M. J., and McCammon, J. A. (2001) Electrostatics of nanosystems: Application to microtubules and the ribosome. *Proc. Natl. Acad. Sci. U. S. A. 98*, 10037−10041.
(44) Humphrey, W., Dalke, A., and Schulten, K. (1996) VMD: visual molecular dynamics. *J. Mol. Graphics 14*, 33−38.
(45) Dolinsky, T. J., Czodrowski, P., Li, H., Nielsen, J. E., Jensen, J. H., Klebe, G., and Baker, N. A. (2007) PDB2PQR: expanding and upgrading automated preparation of biomolecular structures for molecular simulations. *Nucleic Acids Res. 35*, W522−W525.
(46) Woods, C. J., Malaisree, M., Hannongbua, S., and Mulholland, A. J. (2011) A water-swap reaction coordinate for the calculation of absolute protein-ligand binding free energies. *J. Chem. Phys. 134*, 054114.